npj climate and atmospheric science

www.nature.com/npjclimatsci

ARTICLE OPEN

Check for updates

Heatwave–blocking relation change likely dominates over decrease in blocking frequency under global warming

Pak Wah Chan[1]✉, Jennifer L. Catto[1] and Matthew Collins[1]

Extra-tropical continental summer heatwaves often occur under persistent anticyclones or blocking. Here we partition heatwave changes into contributions from blocking changes, heatwave–blocking relation change and mean temperature increase, under global warming in climate models. We employ an optimized blocking index that best correlates with heatwaves (Pearson correlation of 0.7) and find heatwave-driving blocking decreases but the change in heatwave–blocking relation likely dominates. Over Europe, with a historical heatwave frequency of 2.5%, less blocking will cause 0.6% fewer heatwaves, steepened heatwave–blocking relation will cause 1.4% more heatwaves, and the mean temperature increase will cause 60% more heatwaves. Over Greenland, flattened heatwave–blocking relation will dominate over the insignificant decrease in blocking. The future increase in heatwave frequency is not caused by changes in blocking frequency, but by factors such as thermodynamics, that enhance the capacity of blocking to drive heatwaves.

npj Climate and Atmospheric Science (2022)5:68 ; https://doi.org/10.1038/s41612-022-00290-2

INTRODUCTION

Heatwaves pose substantial threats to human society and will be more frequent under global warming (ref. [1] and references therein). Climate model simulations project the extra-tropical continental summer heatwave frequency (when the temperature exceeds the 90th percentile of the recent past for at least 6 consecutive days) to increase from 2.3% in the recent past to 61% by the end of this century, in the scenario of greatest further global warming of 4.2K (shared socioeconomic pathway 5–8.5 or SSP585, see the section "Methods").

Key factors controlling heatwave frequency include, e.g., the increase in mean temperature[2], soil moisture deficits[3–5], and atmospheric circulation patterns. Regarding atmospheric circulation, studies come to rather divided conclusions on whether future circulation will favour more heatwaves or fewer (references in refs. [1,6–9]). Studies of blocking anticyclones find less blocking and heatwaves thus caused[8]. On the other hand, Mann et al.[10] and Pfleiderer et al.[11] proposed an increase in the occurrence of quasi-resonant amplification events and weakened storm track, suggesting that the circulation will change to favour more heatwaves.

Heatwave-driving circulation systems are often composed of blocking anticyclones[1]—large-scale, quasi-stationary anticyclones that block or divert the jet for extended periods. Blocking anticyclones (or simply 'blocking') drives heatwaves by clear-sky radiative forcing[12], anomalous warm advection[13,14], and subsidence[15]. Given the importance of blocking, the objective of our study is to partition the heatwave changes under future global warming into contributions from blocking changes, changes in heatwave–blocking relation, and mean temperature increase.

RESULTS

An optimized blocking index that best correlates with heatwaves

Blocking may be of different configurations, different amplitudes, different durations, residing over land or ocean, and may or may not lead to heatwaves[14]. Different blocking indices pick different subjective choices of these blocking characteristics (elaborated in subsection "Blocking identification"). Such diversity of blocking indices hinders the future projection of blocking and the heatwaves they drive[14].

Here, we employ the framework first introduced by Chan et al.[16], which is an impact-oriented approach (similar to ref. [17]). That is, we objectively evaluate different subjective choices in blocking characteristics and find the optimized index defining the 'heatwave-driving' blocking that best correlates with summer continental heatwave frequency north of 40°N, where most Northern Hemisphere summer blocking occurs (see the section "Methods" for details).

Unlike Chan et al.[16], which used reanalysis data, we use 13 models from the Coupled Model Intercomparison Project Phase 6 (CMIP6, see the subsection "Data"). CMIP6 gives us more data to make statistically robust conclusions. Also, the future simulations in CMIP6 give us the opportunity to make a quantitative projection of heatwaves and blocking in the warmer future.

We find that the Dole and Gordon[18] index, which identifies persistent positive geopotential anomalies, computed over land points only, with an amplitude threshold of 1.0 standard deviation and duration threshold of 5 days (hereafter 'optimized blocking index') best correlates with summer continental heatwave frequency north of 40°N. The optimized blocking index gives a multi-model-mean cross-validation R^2 of 0.50 (or Pearson correlation r of 0.74) between blocking and heatwaves. The scatter plot from a representative model is shown in Fig. 1. Supplementary Methods discusses how the best correlations between blocking and heatwaves are achieved by (1) excluding blocking over the ocean when continental heatwaves are concerned, (2) tuning the thresholds for amplitude and duration, (3) imposing a duration requirement on each gridpoint to mandate perfect stationarity of blocking, and (4) detecting only anticyclonic anomalies but not mean flow reversals.

[1]College of Engineering, Mathematics and Physical Sciences, University of Exeter, Exeter, UK. ✉email: P.Chan@exeter.ac.uk

Sole effect of blocking changes on heatwave frequency: scalar projection

The optimized blocking index projects a decrease in future blocking frequency when averaged over all Northern Hemisphere land points north of 40°N (Fig. 2a, a multi-model-mean decrease of 1.2% relative to 6.4% in the historical period). We may quantify the sole effect of blocking frequency on future heatwaves and ignore other major factors, by assuming an unchanged heatwave–blocking relationship in the future (change in the relationship will be studied in the subsection "Change in heatwave–blocking relation"). Given a future blocking frequency, we use the linear regression coefficients fitted from the historical data, to project a future heatwave frequency. The uncertainty in so doing is estimated by cross-validation (subsection "Uncertainty estimate") and shown by the error bars in Fig. 1 for one of the models. Averaging all 13 models, the decrease of blocking frequency alone is projected to give a multi-model-mean frequency decrease of 0.4% in heatwave frequency (Fig. 2b), which is one-fifth of the historical frequency of 2.3%. This change occurs when the globe warms by 4.2K (multi-model average) in SSP585 (2060–2099) as compared to historical (1966–2005).

A historical heatwave frequency of 2.3% means that over 40 years (1966–2005) of summer (60 days from 20 June to 18 August), there are, on average, 54 heatwave days over continents north of 40°N. The decrease in heatwave-driving blocking alone is projected to give 10 fewer heatwave days in 40 years in the future (2060–2099). A simple average of 1σ uncertainty of 10-year-mean heatwave frequency is 0.24% (Fig. 2b and see the subsection "Uncertainty estimate").

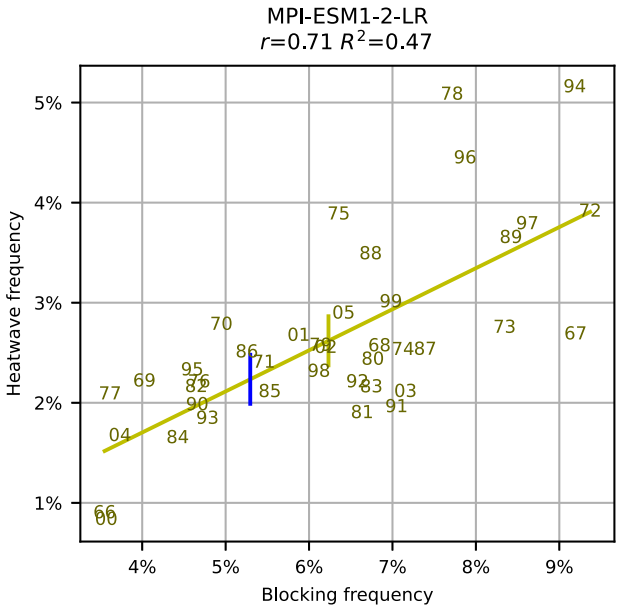

Fig. 1 Optimized blocking index correlates well with heatwave frequency. Scatter plots of heatwave frequency versus optimized blocking index, both averaged over land points north of 40°N, in the MPI-ESM1-2-LR model. Each point represents the mean over one summer (two trailing digits of the year labelled). The ordinary least-squares linear regression line is plotted in yellow. The vertical error bars show the 1σ ranges in estimating the 10-year-mean heatwave frequency using the mean blocking frequency of the historical run (yellow, 1966–2005) and SSP585 run (blue, 2060–2099). r and R^2 are shown (based only on one model and therefore slightly deviate from the multi-model mean).

Sole effect of blocking changes on heatwave frequency: spatial pattern

On the spatial projection of blocking, previous studies have projected a decrease over the North Atlantic and the North Pacific[8,14,19–21] and potentially a localized increase near the Urals (refs. [14,20,21] and references therein). Here, the SSP585 runs together with our optimized blocking index project a decrease in summer blocking frequency in the mid-latitudes and a weaker increase over the Arctic Ocean (Fig. 3c), which is consistent with the poleward shift seen in previous studies (ref. [6] and references therein). The strongest decrease happens over the North Atlantic and the North Pacific, and the decrease near the Urals is not statistically significant (more discussion on the Ural blocking in Supplementary Discussion). Averaging over land points north of 40°N, blocking decreases (see also Fig. 2a). Chan et al.[16] speculated that excluding oceanic blocking might make a difference to future projections of heatwave-driving blocking and here we find that it does not make a qualitative difference.

Figure 3d shows the spatial projection of heatwaves when the linear regression approach is applied to co-located heatwaves and blocking on a coarsened grid (the reduced spatial resolution allows for more robust statistics, due to the infrequent nature of heatwaves). Counting only the effect of blocking frequency, the projection of heatwaves also shows a decrease in the mid-latitudes and a weak increase near the polar regions. Stronger decreases occur along the west coast of continents (the northwest

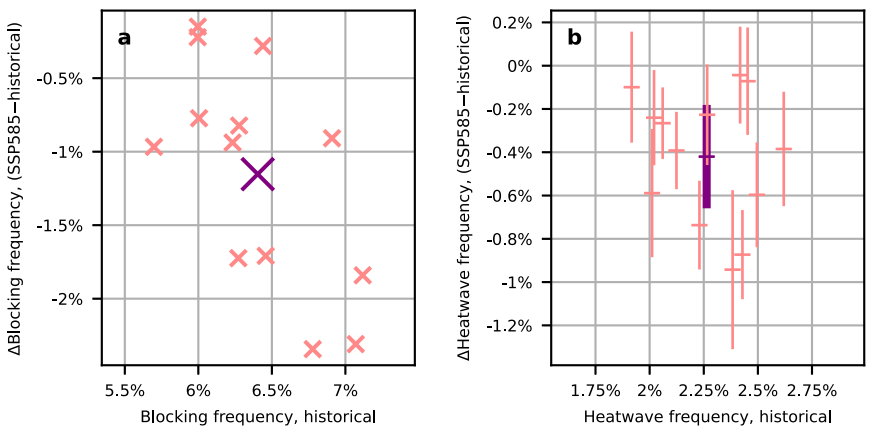

Fig. 2 The decrease of blocking alone is projected to give a one-fifth decrease in heatwave frequency. a Projected change in blocking frequency versus historical blocking frequency. **b** Projected change in heatwave frequency contributed by a change in blocking frequency alone, versus historical heatwave frequency, with 1σ error bars of 10-year-mean heatwave frequency (see the subsection "Uncertainty estimate"). Projections from 13 models are plotted in pink, and a simple arithmetic multi-model mean is plotted in purple. The one-fifth decrease in heatwaves is seen by comparing −0.4% on the y-axis to 2.3% on the x-axis (**b**).

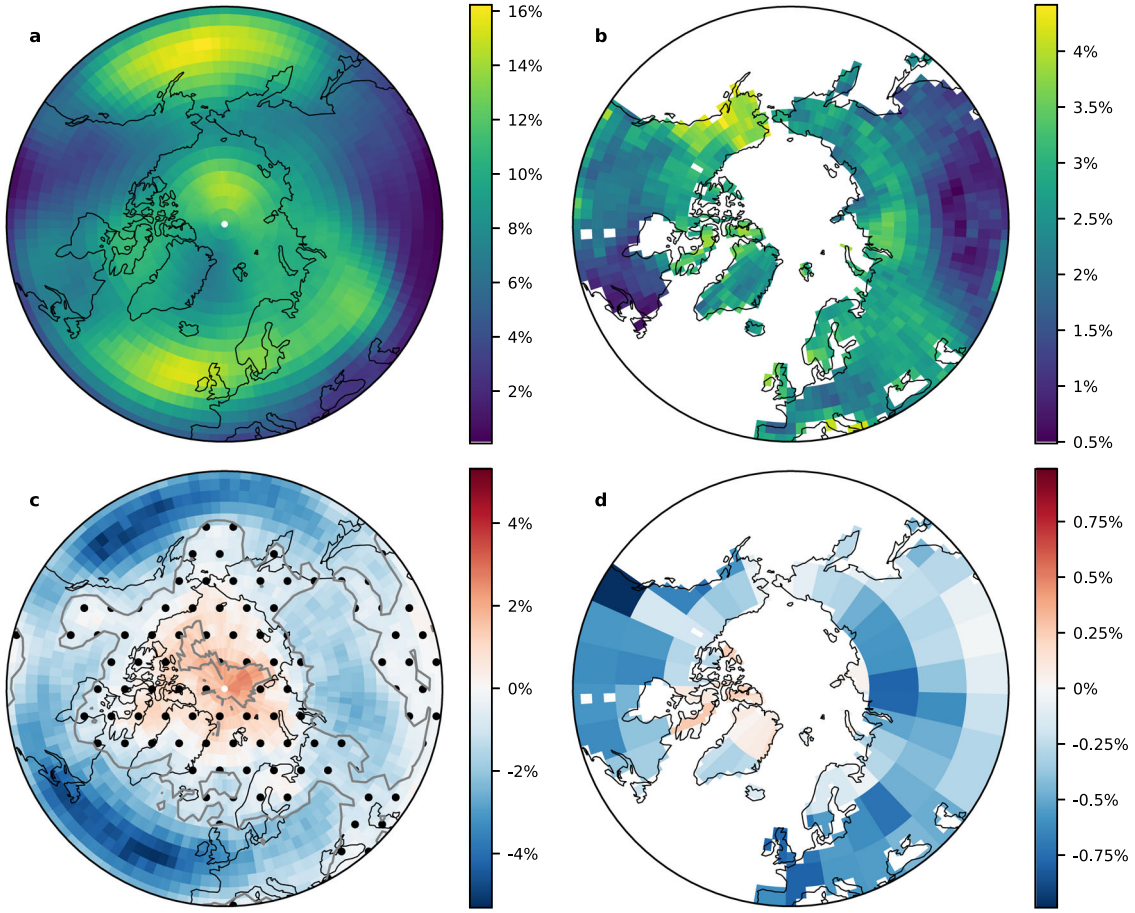

Fig. 3 Spatial projection of summer blocking and heatwaves. a, **b** The multi-model-mean historical (1966–2005) frequency of blocking (**a**) and heatwaves (**b**). **c**, **d** The multi-model-mean frequency change, in SSP585 (2060–2099) minus historical, of blocking (**c**) and heatwaves (**d**, counting only the effect of blocking changes). Dots enclosed in grey contours in **c** denote regions where the changes are NOT statistically significant.

US, the British Isles), central Siberia, and eastern Europe, where the decrease of blocking is strongest.

Change in heatwave–blocking relation

The actual change in heatwave frequency (when the mean temperature increase is removed, Fig. 4) does not resemble the overall decrease considering only the effect of blocking changes (Fig. 3d). Instead, the actual heatwave change is mostly insignificant. This suggests a change in the relationship between heatwaves and blocking. Few regions show significant heatwave change—a significant increase over Europe and a significant decrease over Greenland[2] —which we will study in more detail.

Regarding the change in the heatwave–blocking relation, previous studies[22,23] found no significant change in the heatwave–blocking relation in the future, when heatwaves are calculated relative to the respective climate. Here, we calculate heatwaves relative to the historical percentiles (after removing the mean temperature increase). Over Europe (land points in 40°N–60°N, 10°W–30°E), the linear regression slope between heatwaves and blocking steepens statistically significantly (Fig. 5b), indicating a higher frequency of heatwaves for the same frequency of blocking. The steepened heatwave–blocking relation could be a result of depleted soil moisture and enhanced land–atmosphere coupling[3–5], which enhance the capacity of blocking in driving heatwaves. Over Greenland (land points in

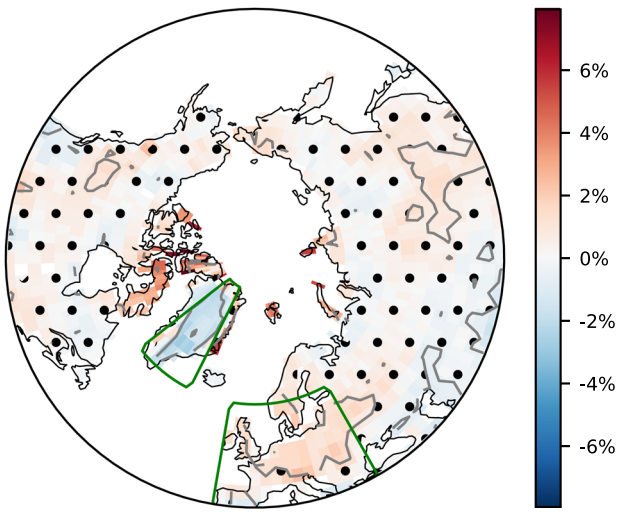

Fig. 4 Few regions show significant heatwave change on top of the mean temperature increase. Shadings show the multi-model-mean change in heatwave frequency when mean temperature increase is removed, in SSP585 (2060–2099) minus historical (1966–2005). Dots enclosed in grey contours denote regions where the changes are NOT statistically significant. Europe and Greenland (land points in green boxes) are studied in more detail.

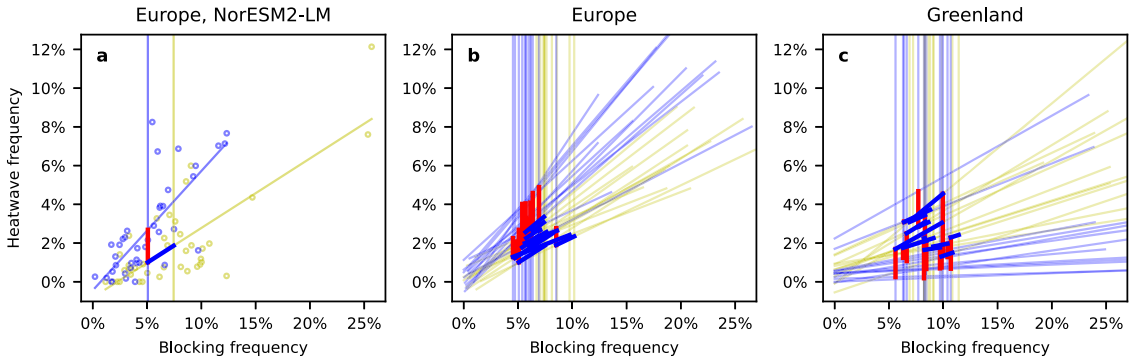

Fig. 5 Sole effect of blocking decrease dominated by the change in heatwave–blocking relation. a Scatter plot of heatwave frequency versus optimized blocking index, both averaged over Europe (land points in 40°N–60°N, 10°W–30°E) for historical (1966–2005, yellow) and SSP585 (2060–2099, blue), in the NorESM2-LM model. Also shown are the mean blocking frequencies (vertical lines) and linear regression lines. Bold line segments show how heatwave changes are contributed by blocking changes (blue) and heatwave–blocking relation change (red). **b**, **c** As **a**, but for 13 CMIP6 models over Europe (**b**) and Greenland (**c**, land points in 60°N–84°N, 52°W–27°W). Individual plots for 13 models are in Supplementary Figs. 1 and 2.

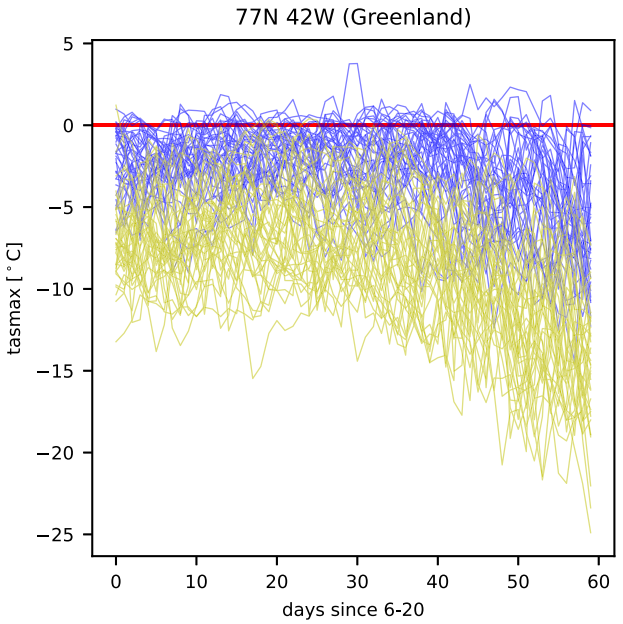

Fig. 6 Ice melting limits temperature variability in future Greenland summer. Time series of daily maximum near-surface temperature (tasmax) at a grid point over Greenland in the ACCESS-CM2 model, for historical (yellow, 1966–2005) and SSP585 (blue, 2060–2099). The red line marks the ice melting point.

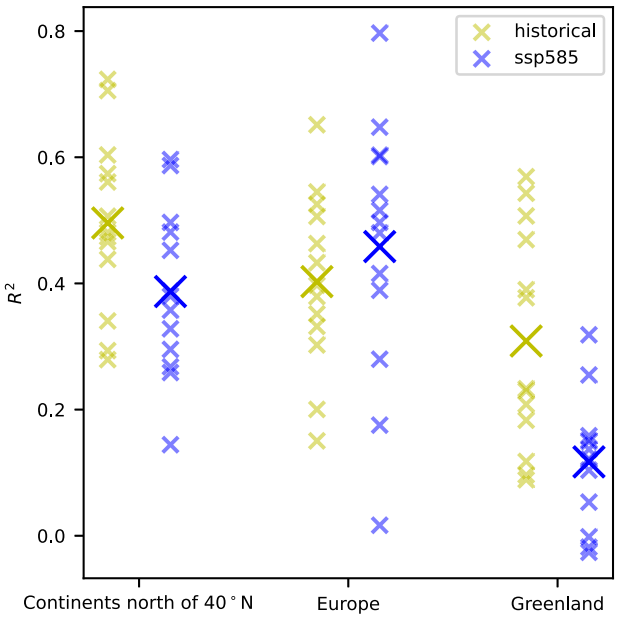

Fig. 7 Correlation between heatwaves and blocking varies insignificantly in the future over continents north of 40°N and Europe. Cross-validation R^2 of 13 CMIP6 models over different regions are shown for historical (yellow, 1966–2005) and SSP585 (blue, 2060–2099). Bigger crosses show the multi-model mean. R^2 decreases significantly in the future over Greenland, perhaps because of the scarcity of future heatwaves.

60°N–84°N, 52°W–27°W), the heatwave–blocking slope decreases significantly (Fig. 5c). The temperature there will be less negative in the future warmer summers. The melting of ice, which requires the absorption of latent heat, will occur more frequently and limit the temperature variability and blocking's capacity in driving heatwaves (Fig. 6).

Over Europe, though the heatwave–blocking slope increases significantly, the correlation between heatwaves and blocking varies insignificantly in the future (Fig. 7), and it is still the same type of blocking anticyclones (i.e., measured with the same amplitude threshold of 1.0 standard deviation and duration threshold of 5–6 days) that best correlates with heatwaves, which is in contrast with ref. [24]. Over Greenland, the heatwave–blocking correlation decreases significantly, perhaps because of the scarcity of future heatwaves. Note that the large spread in heatwave–blocking correlation among models (Fig. 7) unlikely comes from model biases, as the inter-model variations of R^2 in historical do not correlate with those in SSP585. Instead, the large spread in R^2 may come from random sampling, as supported by a similarly large spread in correlation being also found among different realizations of the same model (Table 2 in ref. [23]).

Putting different factors together, over Europe, with an average historical heatwave frequency of 2.5%, the steepened heatwave–blocking relation causes, on average, a 1.4% increase in heatwave frequency (the bold red line segments in Fig. 5b). This overwhelms the effect of blocking frequency decrease (0.6% decrease in heatwave frequency on average, the bold blue line segments in Fig. 5b). Over Greenland, with historical heatwave frequency of 2.6%, the flattened heatwave–blocking relation will cause a 1.1% decrease in heatwave frequency (Fig. 5c). This

dominates over the effect of insignificant blocking frequency decrease (0.1% decrease in heatwave frequency, Fig. 5c).

DISCUSSION

Blocking plays a crucial role in driving heatwaves. To quantify the effect of blocking changes on heatwave frequency, we find an optimized blocking index defining 'heatwave-driving blocking' that best correlates with summer continental heatwave frequency north of 40°N. The optimized blocking index gives a multi-model-mean cross-validation R^2 of 0.50 (or Pearson correlation of 0.74) between blocking and heatwaves.

For continents north of 40°N, applying the optimized blocking index to 13 CMIP6 models simulating SSP585 (2060–2099, scenario of the greatest future warming of 4.2K), we find that the average frequency of heatwave-driving blocking will drop by 1.2%, from 6.4% in the historical period. Counting only the effect of less heatwave-driving blocking, heatwave frequency will be one-fifth less (Fig. 2b, a frequency decrease of $0.4 \pm 0.2\%$ in comparison with the historical frequency of 2.3%). The simple 1σ uncertainty in projecting the 10-year-mean heatwave frequency is 0.24%.

Interesting though in Europe, the heatwave–blocking slope steepens significantly in the future (Fig. 5b) while the heatwave–blocking correlation varies insignificantly (Fig. 7). The increase in heatwave frequency is partitioned into 1.4% increase from the change in heatwave–blocking relation, 0.6% decrease from less blocking, and about 60% increase from the mean temperature increase. Over Greenland, the heatwave–blocking slope flattens significantly in the future (Fig. 5c). The increase in heatwave frequency is partitioned into a 1.1% decrease from the change in heatwave–blocking relation, 0.1% decrease from insignificantly less blocking, and 71% increase from the mean temperature increase. Hence, apart from the mean temperature increase and the change in the seasonal cycle[2,25], there are still important thermodynamic factors that enhance the capacity of blocking to drive heatwaves, e.g., depleted soil moisture and enhanced land–atmosphere coupling[3–5] that dominate the trends. Therefore, studies are needed to better understand the enhancing factors that cause a steepened heatwave–blocking relation.

The decrease in blocking we find is in line with the emerging consensus that blocking will decrease with global warming[8], and the argument that blocking decreases with Arctic amplification as the variance of 500-hPa height (zg500) decreases[26,27]. However, the decrease is in contrast with studies suggesting that circulation will change in a way favoring more heatwaves under global warming[10,11,28–30]. Some of those studies included the increase in zg500 mean state[29,30], which is excluded in this study. Some studies considered other circulation patterns conducive to heatwaves, e.g., quasi-resonant amplification events[10] and a weakened storm track[11]. A rigorous comparison of different heatwave-conducive circulation patterns is still needed[9].

Note that our optimized blocking index measures the variability of zg500, which might not be purely dynamic but influenced by thermodynamic factors like soil moisture[31]. But in the climate model projections, even when soil moisture is projected to decrease (which tends to increase zg500 variability), the zg500 variability is actually projected to decrease. This would suggest an inherent decrease in the dynamic effect. Also, note that this study only looks into the frequency of blocking and heatwaves each using one single duration threshold and no size threshold. So, it is only a bulk summary and may not fit all purposes in measuring impact, especially when blocking duration or size may change under climate change[32].

The framework introduced here can well be used to study other types of weather extremes that are associated with blocking, such as cold spells and heavy precipitation.

METHODS

Data

We use 40 years each from 'historical' (1966–2005) and 'SSP585' (2060–2099) runs in Coupled Model Intercomparison Project Phase 6 (CMIP6)[33]. Daily maximum near-surface temperatures (tasmax) are used to identify heatwaves, and daily 500-hPa geopotential heights (zg500) are used to identify blocking. We also use monthly near-surface temperature (tas) and find that the global mean temperature is 4.2 K higher in SSP585 than historical (recent past, not pre-industrial, multi-model mean).

Thirteen models (ACCESS-CM2, CMCC-ESM2, CNRM-CM6-1, CNRM-ESM2-1, CanESM5, EC-Earth3-Veg-LR, HadGEM3-GC31-LL, HadGEM3-GC31-MM, IPSL-CM6A-LR, MIROC-ES2L, MPI-ESM1-2-LR, NorESM2-LM, UKESM1-0-LL) have the desired variables at the desired frequency, and the first variant_label from each model is used in this study. All variables are first regridded to a 128×64 Gaussian grid (approximately 2.8° resolution).

We focus on areas north of 40°N, where summer blocking often occurs. Following Chan et al.[16], we focus on 20 June to 18 August (simply referred to as 'summer'), which are the hottest 60 days for continental areas north of 40°N[16] (see also ref. [34]).

Heatwave identification

Following Chan et al.[16], we first remove the seasonal cycle and long-term trend from daily maximum near-surface temperatures (tasmax), by subtracting 29-day × 11-year moving averages. Eleven years are equally weighted, while the moving averages for 29 days are done by $T_{\mathrm{smth}} = \mathrm{movmean}(\mathrm{movmean}(T))$, where function movmean is a 15-day equally-weighted moving average defined as $\mathrm{movmean}(T) = \sum_{\Delta t=-7}^{7} T_{\Delta t}/15$, where Δt is the relative time in days. Two successive 15-day moving averages will effectively involve 29 days of data in the averaging as follows:

$$\mathrm{movmean}(\mathrm{movmean}(T)) = \sum_{\Delta t=-14}^{14} \frac{15 - |\Delta t|}{225} T_{\Delta t}. \quad (1)$$

This approach removes the seasonal cycle thoroughly, by allowing the seasonal cycle to slowly vary from year to year. By removing the seasonal cycle from the anomalies, the change of the seasonal cycle is not considered as a change in variability[25], but a change in the mean[2]. Following the warm spell duration index (WSDI)[35], heatwaves are defined as tasmax > 90th percentile for at least 6 consecutive days. The percentiles in the respective 'historical' data are used, and the bootstrap procedure[36] is used in the 'historical' period. Finally, summer-averaged heatwave frequencies are averaged over continents north of 40°N to obtain a time series of interannual variations. Multi-model-mean heatwave frequency is 2.3% in historical, and 61% in SSP585 if the mean summer temperature increase is added.

Blocking identification

There are some subjective choices in measuring blocking ('blocking index'), e.g., meteorological variables to use, features to detect, parameters and thresholds, quasi-stationarity criteria and how spatial maps are presented[14,16,19,37]. Briefly, regarding meteorological variables, some use 500-hPa geopotential height; some use vertically averaged potential vorticity (PV); some use potential temperature on 2-PV-unit surface. For features to detect, some detect strong anticyclonic anomaly; some detect reversal of the mean flow; some detect both of them. Blocking indices also have some parameters and thresholds, such as amplitude threshold and duration threshold, which are often subjectively chosen. Blocking indices have different ways of ensuring that blocking is quasi-stationary. Some require perfect stationarity by imposing the duration requirement gridpoint by gridpoint (e.g., ref. [18]). Some only require quasi-stationarity by imposing the duration requirement and overlapping requirement to a contiguous group of gridpoints (e.g., refs. [19,38]). Spatial maps of blocking frequencies are reported in different ways. Some report the hemispheric average (e.g., refs. [19,27,39,40]). Some report on several preferred locations of blocking (e.g., ref. [40]). Some only report on continents[41]. With such a variety, it is not surprising that blocking indices do not give consistent statistics[14,16,19,42]. Nevertheless, these indices are used to draw important conclusions about future changes in weather extremes and underlying dynamics[27,43–45], even though their correlation with weather extremes has rarely been evaluated.

Supplementary Methods study four of these subjective choices in blocking indices, namely, features to detect, parameters and thresholds, quasi-stationarity criteria, and how spatial maps are presented. We do not

Table 1. Blocking indices compared.

Blocking indices	Features to detect	Parameters and thresholds[a]	Stationarity criteria
Dole and Gordon[18] (DG83)[b]	Anomaly	*A* and *D*	Perfect stationarity
Dunn-Sigouin et al.[38] (D13)	Anomaly and mean flow reversal	*A*, *S* and *D*	Quasi-stationarity
Anomaly-only D13	Anomaly	*A*, *S* and *D*	Quasi-stationarity

[a]*A*, *S* and *D* stand for amplitude, spatial-scale and duration thresholds, respectively.
[b]DG83 with $A = 1.0$ standard deviation and $D = 5$ days is the optimized blocking index.

study choices on meteorological variables and use only 500-hPa geopotential height (zg500) because PV diagnostics are not commonly available in CMIP6 data. We select two zg500-based two-dimensional blocking indices from Dole and Gordon[18] (DG83) and Dunn-Sigouin et al.[38] (D13), which correlate better with heatwaves than some other indices[16]. We also create an anomaly-only version of D13, in which we remove the reversal requirement (Table 1).

For all indices, anomalies of zg500 are calculated first by subtracting the 29-day × 11-year moving averages as described in the subsection "Heatwave identification". These anomalies are then scaled by $\sin 45^\circ / \sin \phi$ following Eq. (1) in Dole and Gordon[18]. Next, the scaled anomalies are normalized by the standard deviation (in the respective 'historical' data, unless otherwise specified). Specifically, the standard deviation is a model-specific scalar calculated as the 5-day-moving mean of area-weighted root-mean-square of the 40-year standard deviation of scaled zg500 anomalies, over all gridpoints north of 40°N. After that, the normalized scaled anomalies go through each of the blocking indices. Finally, summer-averaged blocking frequencies are averaged north of 40°N to give time series of interannual variations.

Measuring the correlation between blocking and heatwaves

To measure the association between blocking and heatwaves, we recall that our objective is to quantify the sole effect of blocking changes on heatwaves under future global warming. Concretely, we want to provide a quantitative projection of future heatwaves, when future blocking statistics are given (by CMIP6). The association between blocking and heatwaves (or extremes in general) has previously been studied using case studies (e.g., ref. [46]), composite analysis (e.g., refs. [15,47]), probability of detection[12], odds ratio[48], and Spearman's rank correlation[23]. These approaches have difficulties in getting a quantitative projection of future heatwaves, or an uncertainty estimate of such a projection.

This study follows Chan et al.[16] in using linear regression, which is a simple approach that provides a quantitative projection of future heatwave frequency when future blocking frequency is given. We consider this problem as a 'model selection' problem in statistics and machine learning, where we are selecting a blocking index, trained by the 'historical' data and projecting into the 'SSP585' period. For this out-of-sample prediction problem, we use cross-validation, as it can avoid over-fitting features that do not robustly recur in the training data. Four-fold cross-validation is conducted 50 times. Each time the data are randomly permutated and split into four subsets ('folds') of 10 years. Holding out one fold for validation, interannual variations of heatwave frequency are linearly regressed on interannual variations of blocking frequency over the other three folds of training data. Because we are interested in a time scale of 10 or more years, the validation is to calculate the squared difference between the 10-year-mean heatwave frequency (mean of the validation fold) and the projection using the 10-year-mean blocking frequency. We use 'MSE' to denote the mean of the 200 squared differences, from 50 times of four-fold cross-validation.

For easier comprehension, we normalize and convert MSE to R^2 as follows. We calculate a baseline MSE like the above procedure, but instead of using blocking data, we simply project heatwave frequency to be the mean in training data, not to fit the linear regression slope against blocking. We calculate R^2 as

$$R^2 = 1 - \frac{\mathrm{MSE}}{\mathrm{MSE}_{\mathrm{baseline}}}. \quad (2)$$

The R^2 is similar to, and usually slightly smaller than the square of the Pearson correlation (denoted as r^2 in small letter), because the cross-validation R^2 measures out-of-sample validation error while the Pearson correlation measures in-sample training error. The square of Pearson correlation r^2 cannot be negative, but the cross-validation R^2 can be negative if blocking correlates poorly with heatwaves. In such cases, fitting the linear regression slope gives extra variability and thus a higher MSE than the baseline MSE, which does not fit the linear regression slope. Chan et al.[16] also normalized the cross-validation MSE similarly, and the e^2 in their study is converted to R^2 as $R^2 = 1 - e^2$.

We process each model separately and average together the R^2, without assuming inter-model correlation. To test the statistical significance of one blocking index giving higher R^2 than another, we do a *t*-test on the 13 paired differences of R^2 from the 13 models, to test whether their mean deviates from zero.

Uncertainty estimate

The square root of MSE is our 1σ estimate of uncertainty when 30 years are used in training to project a 10-year-mean heatwave frequency. The uncertainty will be smaller if we are projecting the mean of more years, or if we use more years in training. This uncertainty reflects only the uncertainty of the linear regression coefficients, but not the uncertainty in blocking frequency, nor the uncertainty in the optimized thresholds (because the thresholds are hyper-parameters in the cross-validation). The bold purple error bar in Fig. 2b shows the simple arithmetic mean of the 13 error bars. So the uncertainty does not include the inter-model spread, nor decrease due to a multi-model approach.

DATA AVAILABILITY

CMIP6 model data are available from https://esgf-node.llnl.gov/projects/cmip6. We acknowledge the World Climate Research Programme, which, through its Working Group on Coupled Modelling, coordinated and promoted CMIP6. We thank the climate modelling groups for producing and making available their model output, the Earth System Grid Federation (ESGF) for archiving the data and providing access, and the multiple funding agencies that support CMIP6 and ESGF.

CODE AVAILABILITY

Computer code to repeat the results is available on Zenodo[49]. The D13 blocking index code is provided by Etienne Dunn-Sigouin. This study uses xarray[50] and scikit-learn[51].

Received: 7 December 2021; Accepted: 1 August 2022;
Published online: 01 September 2022

REFERENCES

1. Perkins, S. E. A review on the scientific understanding of heatwaves—their measurement, driving mechanisms, and changes at the global scale. *Atmos. Res.* **164–165**, 242–267 (2015).
2. Argüeso, D., Di Luca, A., Perkins-Kirkpatrick, S. E. & Evans, J. P. Seasonal mean temperature changes control future heat waves. *Geophys. Res. Lett.* **43**, 7653–7660 (2016).
3. Schär, C. et al. The role of increasing temperature variability in European summer heatwaves. *Nature* **427**, 332–336 (2004).
4. Seneviratne, S. I., Lüthi, D., Litschi, M. & Schär, C. Land–atmosphere coupling and climate change in Europe. *Nature* **443**, 205–209 (2006).
5. Chan, D., Rigden, A., Proctor, J., Chan, P. W. & Huybers, P. Differences in radiative forcing, not sensitivity, explain differences in summertime land temperature variance change between CMIP5 and CMIP6. *Earth's Future* **10**, e2021EF002402 (2022).

6. Kautz, L.-A. et al. Atmospheric blocking and weather extremes over the Euro-Atlantic sector—a review. *Weather Clim. Dyn.* **3**, 305–336 (2022).
7. Coumou, D., Di Capua, G., Vavrus, S., Wang, L. & Wang, S. The influence of Arctic amplification on mid-latitude summer circulation. *Nat. Commun.* **9**, 2959 (2018).
8. Hoskins, B. & Woollings, T. Persistent extratropical regimes and climate extremes. *Curr. Clim. Chang. Rep.* **1**, 115–124 (2015).
9. Huguenin, M. F. et al. Lack of change in the projected frequency and persistence of atmospheric circulation types over Central Europe. *Geophys. Res. Lett.* **47**, e2019GL086132 (2020).
10. Mann, M. E. et al. Projected changes in persistent extreme summer weather events: the role of quasi-resonant amplification. *Sci. Adv.* **4**, eaat3272 (2018).
11. Pfleiderer, P., Schleussner, C.-F., Kornhuber, K. & Coumou, D. Summer weather becomes more persistent in a 2 °C world. *Nat. Clim. Change* **9**, 666–671 (2019).
12. Pfahl, S. & Wernli, H. Quantifying the relevance of atmospheric blocking for co-located temperature extremes in the Northern Hemisphere on (sub-)daily time scales. *Geophys. Res. Lett.* **39**, L12807 (2012).
13. Miralles, D. G., Teuling, A. J., Van Heerwaarden, C. C. & de Arellano, J. V.-G. Mega-heatwave temperatures due to combined soil desiccation and atmospheric heat accumulation. *Nat. Geosci.* **7**, 345–349 (2014).
14. Woollings, T. et al. Blocking and its response to climate change. *Curr. Clim. Chang. Rep.* **4**, 287–300 (2018).
15. Nabizadeh, E., Lubis, S. W. & Hassanzadeh, P. The 3D structure of Northern Hemisphere blocking events: climatology, role of moisture, and response to climate change. *J. Clim.* **34**, 9837–9860 (2021).
16. Chan, P.-W., Hassanzadeh, P. & Kuang, Z. Evaluating indices of blocking anticyclones in terms of their linear relations with surface hot extremes. *Geophys. Res. Lett.* **46**, 4904–4912 (2019).
17. Yau, A. M.-W. & Chang, E. K.-M. Finding storm track activity metrics that are highly correlated with weather impacts. Part I: Frameworks for evaluation and accumulated track activity. *J. Clim.* **33**, 10169–10186 (2020).
18. Dole, R. M. & Gordon, N. D. Persistent anomalies of the extratropical Northern Hemisphere wintertime circulation: geographical distribution and regional persistence characteristics. *Mon. Weather Rev.* **111**, 1567–1586 (1983).
19. Barnes, E. A., Slingo, J. & Woollings, T. A methodology for the comparison of blocking climatologies across indices, models and climate scenarios. *Clim. Dyn.* **38**, 2467–2481 (2012).
20. Dunn-Sigouin, E. & Son, S.-W. Northern Hemisphere blocking frequency and duration in the CMIP5 models. *J. Geophys. Res. Atmos.* **118**, 1179–1188 (2013).
21. Masato, G., Hoskins, B. J. & Woollings, T. Winter and summer Northern Hemisphere blocking in CMIP5 models. *J. Clim.* **26**, 7044–7059 (2013).
22. Brunner, L., Schaller, N., Anstey, J., Sillmann, J. & Steiner, A. K. Dependence of present and future European temperature extremes on the location of atmospheric blocking. *Geophys. Res. Lett.* **45**, 6311–6320 (2018).
23. Schaller, N. et al. Influence of blocking on Northern European and Western Russian heatwaves in large climate model ensembles. *Environ. Res. Lett.* **13**, 054015 (2018).
24. Jézéquel, A. et al. Conditional and residual trends of singular hot days in Europe. *Environ. Res. Lett.* **15**, 064018 (2020).
25. Fischer, E. M. & Schär, C. Future changes in daily summer temperature variability: driving processes and role for temperature extremes. *Clim. Dyn.* **33**, 917–935 (2009).
26. Hassanzadeh, P., Kuang, Z. & Farrell, B. F. Responses of midlatitude blocks and wave amplitude to changes in the meridional temperature gradient in an idealized dry GCM. *Geophys. Res. Lett.* **41**, 5223–5232 (2014).
27. Hassanzadeh, P. & Kuang, Z. Blocking variability: Arctic amplification versus Arctic Oscillation. *Geophys. Res. Lett.* **42**, 8586–8595 (2015).
28. Horton, D. E. et al. Contribution of changes in atmospheric circulation patterns to extreme temperature trends. *Nature* **522**, 465–469 (2015).
29. Diffenbaugh, N. S. & Ashfaq, M. Intensification of hot extremes in the United States. *Geophys. Res. Lett.* **37**, L15701 (2010).
30. Meehl, G. A. & Tebaldi, C. More intense, more frequent, and longer lasting heat waves in the 21st century. *Science* **305**, 994–997 (2004).
31. Fischer, E. M., Seneviratne, S. I., Vidale, P. L., Lüthi, D. & Schär, C. Soil moisture–atmosphere interactions during the 2003 European summer heat wave. *J. Clim.* **20**, 5081–5099 (2007).
32. Nabizadeh, E., Hassanzadeh, P., Yang, D. & Barnes, E. A. Size of the atmospheric blocking events: scaling law and response to climate change. *Geophys. Res. Lett.* **46**, 13488–13499 (2019).
33. Eyring, V. et al. Overview of the Coupled Model Intercomparison Project Phase 6 (CMIP6) experimental design and organization. *Geosci. Model Dev.* **9**, 1937–1958 (2016).
34. McKinnon, K. A., Rhines, A., Tingley, M. P. & Huybers, P. Long-lead predictions of eastern United States hot days from Pacific sea surface temperatures. *Nat. Geosci.* **9**, 389–394 (2016).
35. Alexander, L. V. et al. Global observed changes in daily climate extremes of temperature and precipitation. *J. Geophys. Res.* **111**, D05109 (2006).
36. Zhang, X., Hegerl, G., Zwiers, F. W. & Kenyon, J. Avoiding inhomogeneity in percentile-based indices of temperature extremes. *J. Clim.* **18**, 1641–1651 (2005).
37. Barriopedro, D., García-Herrera, R. & Trigo, R. M. Application of blocking diagnosis methods to General Circulation Models. Part I: a novel detection scheme. *Clim. Dyn.* **35**, 1373–1391 (2010).
38. Dunn-Sigouin, E., Son, S.-W. & Lin, H. Evaluation of Northern Hemisphere blocking climatology in the global environment multiscale model. *Mon. Weather Rev.* **141**, 707–727 (2013).
39. Francis, J. A. & Vavrus, S. J. Evidence for a wavier jet stream in response to rapid Arctic warming. *Environ. Res. Lett.* **10**, 014005 (2015).
40. Martineau, P., Chen, G. & Burrows, D. A. Wave events: climatology, trends, and relationship to Northern Hemisphere winter blocking and weather extremes. *J. Clim.* **30**, 5675–5697 (2017).
41. Liu, J., Curry, J. A., Wang, H., Song, M. & Horton, R. M. Impact of declining Arctic sea ice on winter snowfall. *Proc. Natl Acad. Sci. USA* **109**, 4074–4079 (2012).
42. Barnes, E. A., Dunn-Sigouin, E., Masato, G. & Woollings, T. Exploring recent trends in Northern Hemisphere blocking. *Geophys. Res. Lett.* **41**, 638–644 (2014).
43. Barnes, E. A. & Screen, J. A. The impact of Arctic warming on the midlatitude jet-stream: Can it? Has it? Will it? *Wiley Interdiscip. Rev. Clim. Chang.* **6**, 277–286 (2015).
44. Francis, J. A. & Vavrus, S. J. Evidence linking Arctic amplification to extreme weather in mid-latitudes. *Geophys. Res. Lett.* **39**, L06801 (2012).
45. Kug, J.-S. et al. Two distinct influences of Arctic warming on cold winters over North America and East Asia. *Nat. Geosci.* **8**, 759–762 (2015).
46. Dole, R. et al. Was there a basis for anticipating the 2010 Russian heat wave? *Geophys. Res. Lett.* **38**, L06702 (2011).
47. Trigo, R. M., Trigo, I. F., DaCamara, C. C. & Osborn, T. J. Climate impact of the European winter blocking episodes from the NCEP/NCAR reanalyses. *Clim. Dyn.* **23**, 17–28 (2004).
48. Röthlisberger, M., Pfahl, S. & Martius, O. Regional-scale jet waviness modulates the occurrence of midlatitude weather extremes. *Geophys. Res. Lett.* **43**, 10989–10997 (2016).
49. Chan, P. W., Catto, J. L. & Collins, M. PackardChan/ccc2022-heatwave-blocking-CMIP. *Zenodo* https://doi.org/10.5281/zenodo.6820332 (2022)
50. Hoyer, S. & Hamman, J. xarray: N-D labeled arrays and datasets in Python. *J. Open Res. Softw.* **5**, 10 (2017).
51. Pedregosa, F. et al. Scikit-learn: machine learning in Python. *J. Mach. Learn. Res.* **12**, 2825–2830 (2011).

ACKNOWLEDGEMENTS

The authors would like to acknowledge the use of the University of Exeter High-Performance Computing (HPC) facility and the Harvard University FASRC Cannon cluster in carrying out this work. The authors thank Philip Sansom and Duo Chan for fruitful discussions. This work was supported by the Natural Environment Research Council [grant number NE/S004645/1].

AUTHOR CONTRIBUTIONS

P.W.C. designed the study, did the analysis and drafted the paper. J.L.C. and M.C. supervised the study. All authors contributed to the editing of the paper and discussion of the results.

COMPETING INTERESTS

The authors declare no competing interests.

ADDITIONAL INFORMATION

Supplementary information The online version contains supplementary material available at https://doi.org/10.1038/s41612-022-00290-2.

Correspondence and requests for materials should be addressed to Pak Wah Chan.

Reprints and permission information is available at http://www.nature.com/reprints

Publisher's note Springer Nature remains neutral with regard to jurisdictional claims in published maps and institutional affiliations.